

pubs.acs.org/acssensors Article

Harnessing Redox Polymer Dynamics for Enhanced Glucose—Oxygen Coupling in Dual Biosensing and Therapeutic Applications

Wassim El Housseini, Egor Baiarashov, Rokas Gerulskis, Adam Milam, and Shelley D. Minteer*



Cite This: https://doi.org/10.1021/acssensors.4c00685



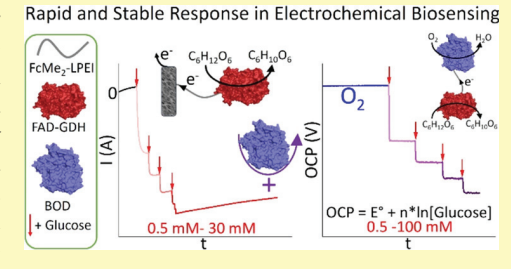
ACCESS

Metrics & More

Article Recommendations

s Supporting Information

ABSTRACT: The burgeoning field of continuous glucose monitoring (CGM) for diabetes management faces significant challenges, particularly in achieving precise and stable biosensor performance under changing environmental conditions such as varying glucose concentrations and O₂ levels. To address this, we present a novel biosensor based on the electroless coupling of glucose oxidation catalyzed by flavin-dependent glucose dehydrogenase (FAD-GDH) and O₂ reduction catalyzed by bilirubin oxidase (BOD) via a redox polymer, dimethylferrocene-modified linear poly(ethylenimine), FcMe₂-LPEI. Initial cyclic voltammetry tests confirm the colocalization of both enzymatic reactions within the potential range of the polymer, indicating an effective electron shuttle mechanism. As a result, we created



a hybrid biosensor that operates at open-circuit potential (OCP). It can detect glucose concentrations of up to 100 mM under various O_2 conditions, including ambient air. This resulted from optimizing the enzyme ratio to $120 \pm 10 \text{ mU}_{BOD} \cdot U_{FAD-GDH}^{-1} \cdot atm_{O_2}^{-1}$. This biosensor is highly sensitive, a crucial feature for CGM applications. This distinguishes it from FAD-GDH traditional biosensors, which require a potential to be applied to measure glucose concentrations up to 30 mM. In addition, this biosensor demonstrates the ability to function as a noninvasive, external device that can adapt to changing glucose levels, paving the way for its use in diabetes care and, potentially, personalized healthcare devices. Furthermore, by leveraging the altered metabolic pathways in tumor cells, this system architecture opened up new avenues for targeted glucose scavenging and O_2 reduction in cancer therapy.

KEYWORDS: redox polymer, glucose oxidation, O₂ reduction, biosensor, electroless coupling

■ INTRODUCTION

Coupling of oxidation and reduction (redox) reactions is a fundamental process underpinning every electrochemical reaction, ranging from energy storage systems, such as batteries and fuel cells, to biosensors and catalysis. 1,2 Redox coupling typically consists of separating the oxidation and reduction reactions on two electrodes separated by a potential-generating device such as a potentiostat. Electroless coupling refers to a system in which electron transfer between coupled redox reactions occurs in a system without the need for separate electrodes or external power sources.³ The electroless coupling of redox reactions has been reported using direct electron transfer systems, particularly in the biosynthesis of pure chemicals.4 This approach has shown significant promise in terms of facilitating direct interactions between redox catalysts, paving the way for more atom economy by using the products of oxidation reactions in reduction processes. However, the investigation of electroless coupling via mediated electron transfer, within the same redox mediator, is not reported in the existing literature. This gap highlights a potential opportunity for novel research, which could lead to novel insights and methodologies in the field of electrochemical biosensing and biosynthesis.

Redox polymers are functionalized with redox-active sites along their backbone or on pendant chains, enabling the shuttle of electrons between chemical species through alternating oxidized and reduced sites (commonly termed self-exchange-based conduction), regulated by environmental conditions such as the pH and electrolyte species. 5-12 Hickey et al. 13 reported FcMe2-LPEI as a redox-active polymer that integrates the electroactive ferrocene component with the structural flexibility of LPEI. 14-16 This polymer has been applied in amperometric biosensors for detecting glucose and lactate, utilizing glucose oxidase (GOx) and lactate oxidase (LOx) as enzymatic catalysts, respectively. The sensitivity achieved with this polymer was reported to be 45 \pm 6 μ A· cm⁻²·mM⁻¹ of the substrate.¹³ However, in glucose biosensing, the presence of interfering substances, e.g., ascorbic acid and acetaminophen, poses a challenge in accurate continuous

Received: March 25, 2024 Revised: May 8, 2024 Accepted: May 16, 2024



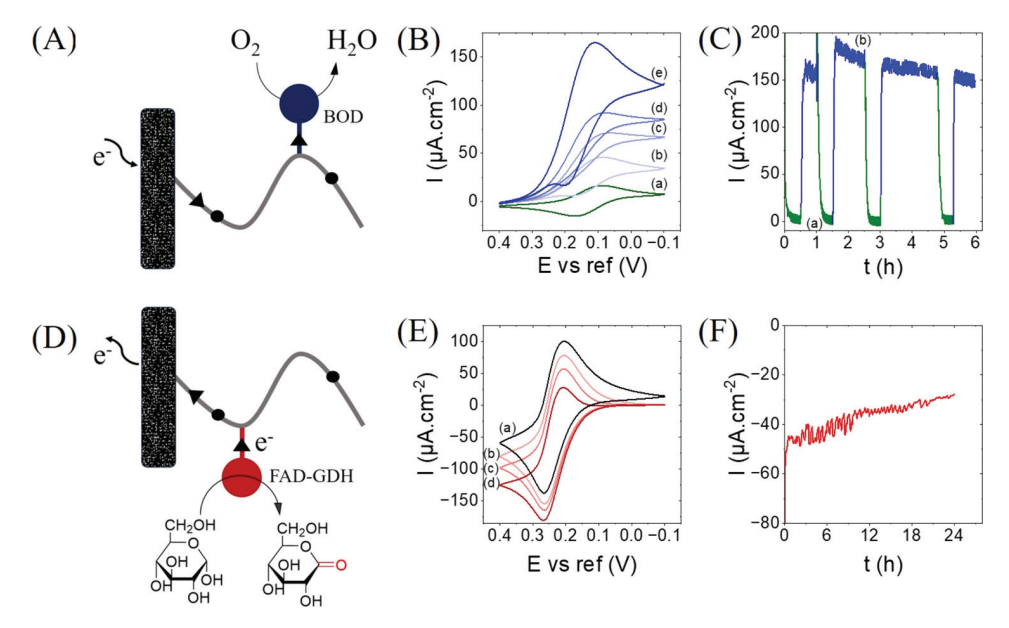


Figure 1. (A) Schematic representation of O₂ reduction electroenzymatically catalyzed by 0.130 U BOD immobilized with FcMe₂-LPEI polymer (BOD@FcMe₂-LPEI) in the presence of EGDGE (serving as a cross-linker). (B) Cyclic voltammetry experiments showing the electroenzymatic activity of BOD@FcMe₂-LPEI in the presence of (a) 0%, (b) 20%, (c) 40%, (d) 60%, and (e) 100% O₂. (C) Bulk electrolysis carried out at 0.1 V vs ref in the presence of (a) N₂ and (b) O₂. (D) Schematic representation of glucose oxidation electroenzymatically catalyzed by 8.100 U FAD-GDH immobilized with the FcMe₂-LPEI polymer (FAD-GDH@FcMe₂-LPEI). (E) Cyclic voltammetry experiments showing the electroenzymatic activity of FAD-GDH@FcMe₂-LPEI in the presence of (a) 0 mM, (b) 5 mM, (c) 10 mM, and (d) 20 mM glucose. (F) Bulk electrolysis carried out at 0.2 V vs ref in the presence of 10 mM glucose and under N₂ bubbling. All experiments were carried out with 100 mM PBS (pH 7.4), at room temperature, and using GCE as the working electrode.

glucose monitoring (CGM), which is one of the key limitations. 17 Typically, an ion-selective membrane, like Nafion, is used to block these interfering substances. 18 Despite this, there is still a significant demand for the development of simpler methods to create sensors that remain unaffected by such substances. In addition, the design of an electrochemical biosensor is crucial as it directly influences the device's ability to transduce biological interactions into measurable electrochemical signals, which are essential for precise and reliable detection in various applications. Effective design can significantly enhance the sensitivity and specificity of biosensors, making them invaluable tools in both research and practical applications. ^{19,20} Consequently, the creation of a glucose biosensor functioning at open-circuit potential (OCP) could notably diminish interference from other electroactive substances found in complex biological fluids. This improvement promises to enhance the accuracy of glucose-level determinations. In addition, this method paves the way for more reliable, and user-friendly glucose monitoring systems, promising significant improvements in diabetes management and other applications requiring precise glucose control.

The central idea of this work is to create an electroless system that couples glucose oxidation to O₂ reduction through a redox polymer. By integrating FcMe₂-LPEI into an enzymatic setup, electron transfer is facilitated between the enzymes involved in glucose oxidation and O₂ reduction reactions without the need for external electrodes or power sources. In glucose oxidation, an enzyme such as flavin-dependent glucose dehydrogenase (FAD-GDH), insensitive to O₂ presence unlike GOx, catalyzes the conversion of glucose into gluconolactone, releasing electrons in the process. Meanwhile, for O₂ reduction, bilirubin oxidase (BOD) can accept these electrons to reduce O₂ molecules to water. The concept of the work revolves in the utilization of OCP as an electroanalytical

technique for glucose detection. This biosensing system distinctively leverages O_2 as a positive factor in the biosensing mechanism, where the changes in OCP are contingent upon the simultaneous presence of both glucose and O_2 only. Such a system could potentially operate continuously as long as substrates, glucose, and O_2 , are available, making it an attractive option for long-term applications in biosensors.²³

In addition to the utility of the electroless coupling system in glucose biosensing, the presented system has 2-fold applicability: as a therapeutic agent in cancer treatment through glucose scavenging, and as a precise O2 filter in electroenzymatic reactions. First, the system can be harnessed for therapeutic purposes in oncology. Tumors often exhibit high glucose and O2 uptake, known as the Warburg effect. 24,25 By scavenging glucose locally, the system could potentially starve cancer cells of the energy required for their growth, while the coupled O2 reduction might amplify the therapeutic effect by modulating the tumor microenvironment, potentially enhancing the efficacy of other treatments.²⁶ Second, in the context of O₂-sensitive electroenzymatic systems, the ability to modulate O₂ levels precisely is of paramount importance. This could be particularly impactful in microfluidic devices²⁷ or bioelectrochemical systems, ^{28–30} where O₂ levels must be lowered to maintain specific reaction conditions and to conserve enzymes electrocatalytic activity.

This work is methodically divided into three main parts, each focusing on a distinct yet interconnected aspect of the electroless coupling of glucose oxidation to O_2 reduction within an electroenzymatic framework. In the first part, we delve into the fundamental electroenzymatic activities of BOD and FAD-GDH, which are instrumental for O_2 reduction and glucose oxidation, respectively, with mediated electron transfer via FcMe₂-LPEI. Then, we employ cyclic voltammetry (CV) experiments to probe the interaction between both enzymes

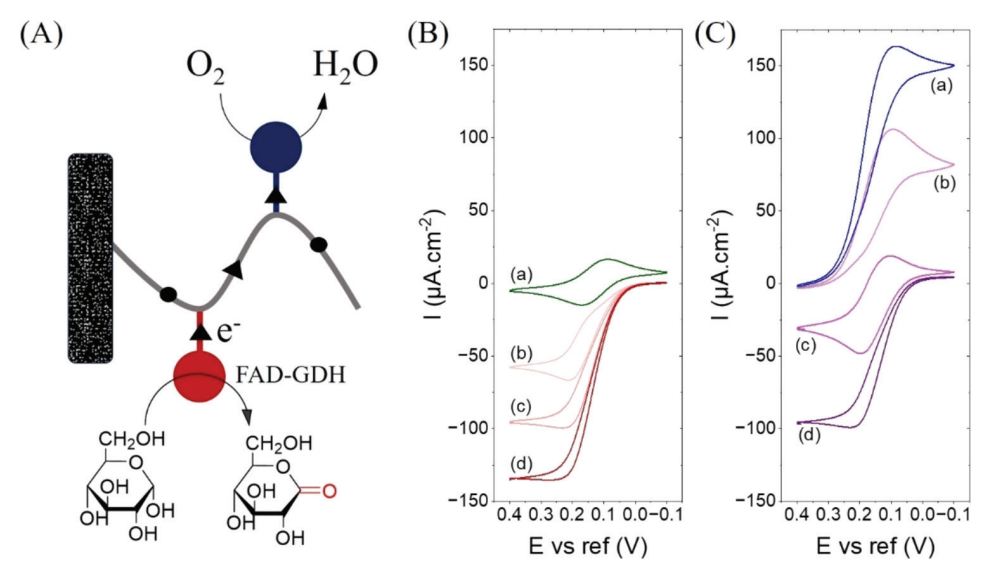


Figure 2. (A) Schematic representation of the electroless coupling between glucose oxidation and O_2 reduction both electroenzymatically catalyzed by 8.100 U FAD-GDH and 0.130 U BOD respectively, and both immobilized with the FcMe₂-LPEI polymer (FAD-GDH/BOD@FcMe₂-LPEI). Cyclic voltammetry experiments with FAD-GDH/BOD@FcMe₂-LPEI under (B) N_2 and (C) O_2 conditions and in the presence of (a) 0 mM, (b) 5 mM, (c) 10 mM, (d) 20 mM glucose. All experiments were carried out with 100 mM PBS (pH 7.4), at room temperature, and using GCE as the working electrode.

and their substrates once immobilized on the same electrode. This initial phase is critical to prove that the electroless coupling between both reactions mediated by the redox polymer is possible. The second part of the study pivots toward the practical application of these insights in the development of a biosensor based on OCP. Finally, we embark on the optimization of the system for the electroless coupling of glucose oxidation with $\rm O_2$ reduction for medical application and $\rm O_2$ filtering. This phase is dedicated to refining the conditions of the system to enhance its efficiency, stability, and overall performance.

RESULTS AND DISCUSSION

Analysis of Electroenzymatic Behaviors of BOD, FAD-GDH, and FAD-GDH/BOD Systems Immobilized with FcMe₂-LPEI. The ability of FcMe₂-LPEI to wire the oxidation of glucose catalyzed by FAD-GDH to the reduction of O₂ catalyzed by BOD, as well as the impact of polymer immobilization on each enzyme's activity was investigated via CV, carried out at 5 mV·s⁻¹, and chronoamperometry (CA). Initially, it was crucial to evaluate the electrocatalytic capabilities of each enzyme individually. A mixture of BOD and FcMe₂-LPEI was cross-linked onto a 3 mm diameter GCE (Figure 1A) to immobilize the enzyme on the electrode and to facilitate surface-to-enzyme electron transfer. The catalytic activity and long-term stability of the film were studied by monitoring the catalytic current density in the absence and presence of O₂.

In the absence of O₂, BOD@FcMe₂-LPEI shows a reversible current arising from the charging of ferrocene moieties on FcMe₂-LPEI (Figure 1B, curve a). In contrast, bubbling the solution with increasing proportions of O₂ showed an increase in the reductive current at 0.1 V vs ref, arising from the electroenzymatic reduction of O₂ catalyzed by BOD@FcMe₂-LPEI. The current density at 0.1 V increased linearly from 0 μ A·cm⁻² at 0% O₂ (20% O₂/80% N₂) (Figure 1B, curve b) to 165 \pm 25 μ A·cm⁻² at 100% O₂ (Figure 1B, curve e).

The observed increase in bioelectrocatalytic activity for O_2 reduction as the concentration of O_2 increases illustrates the effectiveness of BOD@FcMe₂-LPEI in detecting low and high O_2 levels. Additional results concerning the choice of the crosslinking agent and the determination of the optimal duration for cross-linking subsequent to electrode preparation are detailed in the Supporting Material (Part 2). The notable efficacy of BOD in reducing O_2 could be attributed to the effective electron transfer from the polymer to the BOD enzyme. Moreover, the utilization of redox polymers as scaffolds for enzymatic electrodes presents several advantages. A key benefit is their ability to facilitate the addition of multiple enzyme layers on an electrode's surface, significantly boosting the bioelectrocatalytic activity of the system under study.

Furthermore, the bioelectrocatalytic activity and stability of the BOD@FcMe2-LPEI biofilm were further investigated through bulk electrolysis experiments at 0.1 V, both in the absence (section a of Figure 1C) and presence of O₂ (section b of Figure 1C). Under N2 bubbling, the bulk electrolysis curve depicted a current nearly $0 \pm 1 \mu \text{A} \cdot \text{cm}^{-2}$. However, upon switching from N2 to O2, there was a marked increase in the reduction current of O2, reaching a level of approximately 150 \pm 10 μ A·cm⁻². This current density aligns with that observed in the cyclic voltammetry experiments (Figure 1B, curve e). Repeating the procedure of alternating between N₂ and O₂ bubbling demonstrated a consistent pattern of decreasing and increasing in reduction currents, respectively. Notably, under continuous O2 bubbling, the current density exhibited a slight decrease over time, stabilizing at around 125 \pm 21 μ A·cm⁻² after 24 h, which translates to only a 28% loss of current (Figure S4A curve a). This slight reduction in current density might be attributable to the constant bubbling of the solution, potentially causing partial detachment of the biofilm from the electrode surface. This experiment lends further confidence regarding the system's electrocatalytic activity in sensing O2, demonstrating its capability to sustain the electroenzymatic activity effectively over extended periods of operation. Additional results regarding the optimization of bulk

electrolysis experiments are detailed in the Supporting Material (Part 3).

The optimization of the BOD@FcMe2-LPEI system was followed by studying the bioelectrocatalytic oxidation of glucose to gluconolactone catalyzed by FAD-GDH@FcMe2-LPEI, as shown in the schematic representation in Figure 1D. CV experiments were conducted using the same experimental conditions as BOD@Fc-Me2-LPEI. The redox activity of the polymer-enzyme layer was investigated in the absence of glucose (Figure 1E, curve a). Increasing glucose concentration led to an increase in the current emerging from the FAD-GDH-catalyzed oxidation of glucose to gluconolactone. The current density at 0.25 V vs ref increased from 150 \pm 15 μ A· cm^{-2} in the presence of 5 mM glucose (Figure 1E, curve b) to $179 \pm 5 \,\mu\text{A}\cdot\text{cm}^{-2}$ in the presence of 20 mM glucose (Figure 1E, curve d). Furthermore, a bulk electrolysis experiment was carried out at 0.25 V vs ref in the presence of 10 mM glucose. Current density began at $-50 \pm 25 \mu \text{A} \cdot \text{cm}^{-2}$ and decreased gradually to $-30 \pm 11 \ \mu\text{A}\cdot\text{cm}^{-2}$ after 24 h (Figure 1F).

Concurrent voltametric profiles obtained from CV indicate that the redox polymer adeptly mediates both glucose oxidation by GDH and O2 reduction by BOD, occurring within the same potential range. This implies that the redox polymer is capable of effectively bridging the two reactions, affirming the potential of integrating the oxidative and reductive processes in a unified bioelectrocatalytic framework. Following these findings, the subsequent phase of research focused on the dual immobilization of FAD-GDH and BOD together with the polymer on a singular electrode to facilitate simultaneous bioelectrocatalysis. BOD (0.130 U) and FAD-GDH (8.100 U) were both immobilized with FcMe₂-LPEI on the electrode surface as schematically represented in Figure 2A. After 24 h of the electrode preparation, CV experiments were conducted in the presence of glucose and in the presence of N₂ (Figure 2B) and O_2 (Figure 2C).

Under N_2 atmosphere and in the absence of glucose, a reversible redox peak related to the activity of the polymer (Figure 2B, curve a). The addition of increasing amounts of glucose showed a gradual increase in the current density (Figure 2B, curves b (5 mM), c (10 mM), and d (20 mM)). The comparison between FAD-GDH/BOD@FcMe2-LPEI and FAD-GDH@FcMe2-LPEI behavior in the presence of glucose and N_2 obtained shows current densities in the same order of magnitude. For example, in the presence of 20 mM glucose, current densities are equal to -179 ± 5 and $-134 \pm 6 \mu A$ · cm⁻² with FAD-GDH@FcMe2-LPEI (Figure 1E, curve d) and FAD-GDH/BOD@FcMe2-LPEI (Figure 2B, curve d), respectively. This result shows that the interaction between BOD and FAD-GDH on the same electrode does not affect the activity of FAD-GDH.

In addition, the study of the electroenzymatic activity of FAD-GDH/BOD@FcMe₂-LPEI (Figure 2C, curve a) in the presence of 100% O₂ and the absence of glucose shows the electroenzymatic activity of BOD toward O₂ reduction. The addition of 5 mM glucose (Figure 2, curve b) resulted in a decrease of the reduction current, proving the occurrence of both the oxidation of glucose and the reduction of O₂ catalyzed by both enzymes and that takes place in the potential window of the redox polymer. Consequently, the addition of glucose showed a linear decrease in current density with a slope of $-13 \pm 2 \, \mu \text{A} \cdot \text{cm}^{-2} \cdot \text{mM}^{-1}$ glucose. Hence, from CV experiments, the electroless coupling of glucose oxidation to O₂ reduction is successfully taking place in the bioelectrode

system. Furthermore, this phenomenon confirms that the redox polymer successfully facilitates the transfer of electrons between the two enzymes in the presence of their respective substrates.

Exploring OCP-Based Glucose Biosensing. This study focused on the investigation of a biosensor's development. CV experiments have shown that it is possible for glucose oxidation catalyzed by FAD-GDH and O₂ reduction catalyzed by BOD to be coupled without any applied potential. The equilibrium potential at which both reactions are coupled corresponds to the OCP of the reaction. In this case, OCP is determined by the combined thermodynamics of both reactions. In addition, the reactions share common electron transfer without the application of an external potential as previously mentioned. Presented are the equations for the half-reactions, along with an explanation of how the quantities of substrates and enzymes influence the OCP value.

Half-oxidation reaction

$$C_6H_{12}O_6 \rightarrow C_6H_{10}O_6 + 2H^+2e^-$$
 (R1)

$$E_{\text{ox}} = E_{\text{C}_6 \text{H}_{10} \text{O}_6 / \text{C}_6 \text{H}_{12} \text{O}_6}^{\circ} + \frac{0.059}{n} \ln \frac{[\text{C}_6 \text{H}_{12} \text{O}_6]}{[\text{C}_6 \text{H}_{10} \text{O}_6] [\text{H}^+]^2}$$
(E1)

Half-reduction reaction

$$0.5O_2 + 2H^+ + 2e^- \rightarrow H_2O$$
 (R2)

$$E_{\text{red}} = E_{\text{O}_2/\text{H}_2\text{O}}^0 - \frac{0.059}{n} \ln P_{\text{O}_2}^{0.5} [\text{H}^+]^2$$
 (E2)

n is the number of electrons involved in both the oxidation of glucose and in the reduction of O_2 ($n = 2e^-$)

Global reaction

$$C_6H_{12}O_6 + 0.5O_2 \rightarrow C_6H_{10}O_6 + H_2O$$
 (R3)

The overall OCP of the system is not simply the average of the two potentials but is a mixed potential.

$$OCP = OCP_{coupled} = f(E_{red}, E_{ox})$$
 (E3)

f is a function that combines the potential of the two half-reactions. The exact form of f depends on the kinetics and mechanism of electron transfer between the two redox couples

OCP =
$$E^0 - 0.0295 \ln \frac{P_{O_2}^{0.5} \times [C_6 H_{12} O_6]}{[C_6 H_{10} O_6]}$$
 (E4)

$$E^{0} = f(E_{\rm red}^{0}, E_{\rm ox}^{0}) \tag{E5}$$

Initially, the quantity generated of gluconolactone at the beginning of the reaction is insignificant. In consequence, OCP expression is streamlined to

$$OCP = E^{0} - 0.0295 \ln P_{O_{1}}^{0.5} \times [C_{6}H_{12}O_{6}]$$
 (E6)

From (E6), OCP expression will depend on the relative rates and concentrations of the redox species. The biosensor that is being worked on looks into what happens to the OCP values when glucose is added while $\rm O_2$ is present. The main objective of the upcoming section is to verify the viability of this biosensor concept and examine how variations in the quantities of both enzymes affect the accuracy of glucose detection within a specific range of concentrations.

Study of OCP Expression and Its Linearity with Natural Logarithm of Glucose. Before investigating FAD-GDH/BOD@FcMe₂-LPEI electrode capability to detect

ACS Sensors pubs.acs.org/acssensors Article

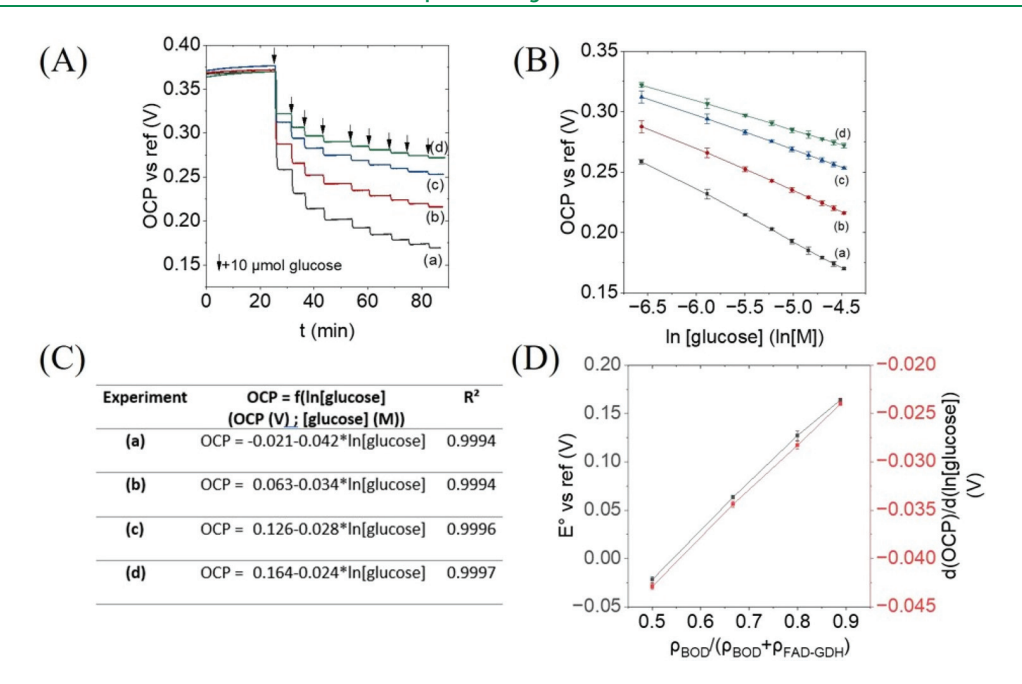


Figure 3. OCP experiments aimed at assessing the performance of a glucose biosensor with a constant amount of BOD and varying amounts of FAD-GDH. (A) Tracking the OCP response over time after successive additions of $10~\mu$ mol glucose, with traces labeled (a–d) corresponding to 0.130 U (6 mg·mL⁻¹) of BOD and different FAD-GDH amounts of 8.100 U (6.00 mg·mL⁻¹), 4.100 U (3 mg·mL⁻¹), 2.050 U (1.50 mg·mL⁻¹), and 1.025 U (0.75 mg·mL⁻¹), respectively, illustrating the dynamic response of the biosensor to changes in glucose levels. (B) Calibration curves and (C) linear relationships linking the OCP response to the natural logarithm of glucose concentration for each BOD and FAD-GDH levels. (D) Plots of the standard potential (E^0) and the sensitivity (d(OCP)/d[ln(glucose)]) against the mass concentration proportion of BOD relative to both enzymes mass concentrations. All experiments were carried out with 100 mM PBS (pH 7.4), at room temperature, under O_2 , with stirring, and using 0.25 cm² carbon paper on which both enzymes were immobilized with FcMe₂-LPEI as the working electrode.

glucose in the presence of O_2 , several control experiments were conducted to ensure accuracy and reliability. Initial examination of the redox polymer solely in the presence of O_2 and subsequent glucose addition revealed no discernible alteration in OCP (Figure S5A). Furthermore, an investigation into the impact of glucose addition on OCP in the presence of O_2 using BOD@FcMe₂-LPEI and FAD-GDH@FcMe₂-LPEI electrodes revealed no discernible effect (Figure S5B,C). Also, looking into how OCP changes for the FAD-GDH/BOD@FcMe₂-LPEI electrode when N_2 is present has not led to any change in OCP (Figure S6). Finally, the investigation into the impact of incorporating the reaction product (gluconolactone) has not revealed any change in OCP (Figure S7).

Figure 3A shows the time course of the continuous measurement of glucose by sequential addition of glucose (between 1 and 11 mM) to the electrolyte solution at a pH of 7.4. Different amounts of both enzymes' mixture were used in this set of experiments where BOD amount was constant 0.130 U (6.00 mg·mL⁻¹) and GDH amount was changed from 8.100 U $(6.00 \text{ mg} \cdot \text{mL}^{-1})$ in experiment (a) to 1.025 U $(0.75 \text{ mg} \cdot$ mL^{-1}) in experiment (d). At around 20 min of O_2 bubbling, corresponding to the saturation of the electrolyte with O_2 , OCP for all studied experiments, where BOD amount was the same (0.130 U), was equal to 0.37 V approximately related to the OCP of the O2 reduction reaction. The addition of 10 $\mu \mathrm{mol}$ of glucose—indicated by the black arrow—resulted in a rapid decrease in OCP as an indication of glucose oxidation reaction. For all conducted experiments, the results showed an immediate and rapid drop in OCP after the addition of glucose, suggestive that the biosensor is sensitive to glucose in the presence of O₂. Systems with a greater quantity of FAD-GDH exhibit a more noticeable drop in OCP because of the

enhanced oxidation rate of glucose. This acceleration in glucose oxidation results in more rapid electron transfer when higher levels of FAD-GDH are present, facilitated by FcMe₂-LPEI. Consequently, this facilitates a more efficient reduction of O₂ by BOD. Subsequent to the observation of the steady-state potential, which indicates sensor recovery and the fulfillment of the natural response for a specific quantity of glucose introduced, further additions of glucose resulted in a more pronounced reduction in OCP (Figure 3A).

Furthermore, the study that looked at what happened when glucose was added at a single point in time (Figure S8, trace c), twice (Figure S8, trace b), or four times (Figure S8, trace a) with the same final concentration of glucose in each experiment shows that the final OCP and the steady-state level were the same in all of them. This experiment demonstrates that the system's response is reproducible and additive to the addition of glucose. In addition, OCP values were derived from the level of stability observed subsequent to the addition of glucose (Plateaus in Figure 3A). An excellent degree of linearity of OCP was observed as a function of the natural logarithmic concentrations of glucose (Figure 3B). The table in Figure 3C illustrates the linear expressions of OCP in relation to ln[glucose] for each of the systems that were investigated. For all systems with different amounts of FAD-GDH presented in Figure 3A, the consistency of the high R^2 , all above 0.9994, indicates an excellent fit across the range of glucose concentrations tested (1-11 mM). As the levels of FAD-GDH decrease, there is an increase in the standard electrode potential (E^0) values; however, the absolute values of the slopes also decrease (table of Figure 3C), signaling a reduction in sensitivity. Despite this, the biosensor still maintains a high degree of sensitivity overall.

ACS Sensors pubs.acs.org/acssensors Article

As obtained in eq (E6), OCP is theoretically influenced by both the logarithm of the glucose concentration and the square root of $\rm O_2$ partial pressure. OCP expression in the table of Figure 3C shows a linear dependency of OCP on the logarithm of glucose concentration. This result suggests that the local $\rm O_2$ pressure variation upon the addition of glucose for the studied system, in Figure 3 (experiments (a–d)), is negligible and that all electrons generated from glucose oxidation are participating in $\rm O_2$ reduction where glucose oxidation is the limiting reaction in the process.

In consequence, eq (E6) can be simplified to (E10)

$$OCP = E_{app}^{0} - 0.0295 \ln([C_6 H_{12} O_6])$$
(E7)

where

$$E_{\rm app}^0 = E^0 - 0.0295 \ln(P_{\rm O_2}^{0.5}) \tag{E8}$$

Under O₂ atmosphere

$$P_{\mathcal{O}_{2}}^{0.5} \cong 1 \text{ atm}; E_{\mathsf{app}}^{0} \cong E^{0}$$
 (E9)

$$OCP = E^{0} - 0.0295 \ln([C_{6}H_{12}O_{6}])$$
 (E10)

Figure 3D shows the evolution of E^0 and the sensitivity of the biosensor as a function of the mass concentration proportion of BOD in the enzymatic mixture. Both OCP expression parameters follow a linearity as a function of BOD's mass concentration proportion. The proportionality indicates that each incremental increase in the proportion mass concentration of BOD leads to a corresponding and predictable increase in E^0 and the sensitivity

$$E^{0} = -0.27 \text{ V} + 0.49 \times (\rho_{\text{BOD}}/(\rho_{\text{BOD}} + \rho_{\text{FAD-GDH}})$$
 (E11)

d(OCP)/d(ln[glucose])

=
$$-0.07 + 0.05 \times (\rho_{BOD}/(\rho_{BOD} + \rho_{FAD-GDH})$$
 (E12)

In addition, a nonlinear relationship was obtained when E^0 and the sensitivity were plotted against the unit proportion of BOD in the mixture (Figure S9B). One potential cause of this nonlinearity could be the kinetic properties of both enzymes where the increase or decrease of enzymatic proportion does not increase or decrease the reaction rate due to substrate saturation or other kinetic limitations. For that, in order to investigate the linear variation of E^0 and sensitivity, the study utilized the mass concentration proportion of either BOD or FAD-GDH. Furthermore, conducting a series of experiments with varying amounts of BOD and FAD-GDH while maintaining the same mass proportion between them yielded noteworthy observations regarding the system's response to glucose in the presence of O2. Regardless of the differing absolute amounts of BOD and FAD-GDH used in each experiment, the decrease in OCP upon the addition of glucose was consistent across all trials (Figure S10A). This indicates a robustness in the system's electrochemical response to glucose, unaffected by the variations in the enzyme quantities as long as their ratio remains constant. Consequently, when analyzing the data by plotting OCP against the natural logarithm of glucose concentration, the extracted values for the standard electrode potential (E^0) and the system's sensitivity are approximately similar (Figure S10B). This result suggests that the ratio of BOD to GDH is a critical factor in maintaining the system's performance, rather than their absolute amounts.

Figure 3 depicts experiments that demonstrate an ideal system, characterized by the linearity of the OCP expression as a function of ln[glucose]. In this system, within the glucose concentration range of 1-11 mM, all electrons generated from glucose oxidation are utilized in reduction processes, and the O₂ pressure changes minimally. On the other hand, the study of the effect of the imbalance in electron transfer was examined. Testing other proportions of BOD and FAD-GDH was investigated where the amount of FAD-GDH was fixed at 8.100 U (6 mg·mL⁻¹) and the amount of BOD was changed (Figure S11A). The amount of BOD was equal to 0.065 U (3.00 mg·mL⁻¹), 0.032 U (1.50 mg·mL⁻¹), 0.016 U (0.75 mg·mL⁻¹) in experiments (a), (b), and (c) respectively. The results show that OCP decreases with successive additions of glucose; however, OCP expression has not followed a linearity with the logarithmic concentration of glucose (Figure S11B) especially with experiment (c) where the amount of BOD is the lowest. When the concentration of GDH is high, the system becomes highly efficient in oxidizing glucose, leading to a rapid generation of electrons. However, the scenario is complicated by the presence of a relatively low amount of BOD. The imbalance arises because the amount of BOD is not sufficient to effectively utilize all of the electrons produced from the oxidation of glucose, especially as the concentration of glucose increases. Since not all electrons are used for O₂ reduction, there will be an accumulation of excess electrons at the electrode. For example, with a very low amount of BOD and a high amount of FAD-GDH, the accumulation of excess electrons leads to a more negative potential at the electrode that potentially increased the OCP with the addition of glucose (Figure S12). In consequence, in order to obtain a linearity in OCP as a function of the natural logarithm of glucose concentration, it is important to make an equilibrium of enzyme amounts or even to use an excess of BOD.

Moving forward, the idea was to detect not only moderate concentrations (1–11 mM) but also low and high concentrations of glucose. The bioelectrode mixture with the lowest amount of FAD-GDH in Figure 3 was utilized to study glucose biosensing across a broad range of concentrations (0.130 U BOD and 1.025 U FAD-GDH). Figure S13A depicts the OCP response over time to different glucose additions (1, 10, and 100 μ mol). As previously observed, OCP decreases with each addition of glucose. The steepest decline is seen when switching from 10 to 100 μ mol glucose additions, indicating the sensor's sensitivity to changes in glucose concentrations. Even with large amounts of glucose added (100 μ mol), OCP reaches a steady state in a short time. The final addition of 100 μ mol of glucose led to a cumulative glucose concentration reaching 100 mM.

Furthermore, after glucose addition, the extracted steady-state OCPs revealed a perfect linear relationship with the natural logarithm of glucose concentration (Figure S13B). This result suggests that, with the optimization of both BOD and FAD-GDH, this biosensor can detect and fit linearly with both low (0.5 mM) and high concentrations of glucose (up to 100 mM). Additionally, experiments with bioelectrode mixtures containing higher proportions of FAD-GDH than those used in this study revealed a nonlinear correlation between OCP and the logarithm of glucose concentration. As previously noted, this nonlinearity is attributed to the swift generation of electrons at higher FAD-GDH levels and high glucose concentrations, exceeding the capacity for $\rm O_2$ reduction

(Figure S14). Therefore, the optimal bioelectrode mixture for glucose biosensing across a broad range, when operating in an $\rm O_2$ environment, is found to be with 0.130 U of BOD and 1.025 U of FAD-GDH.

The study of glucose biosensing using OCP in the presence of O_2 was expanded to include experiments with atmospheric air, where the O_2 proportion is approximately 21%. Similar to the observations made with 100% O_2 , the addition of glucose resulted in a decrease in OCP. After optimizing the enzyme ratio, the OCP response exhibited a linear relationship with the natural logarithm of the glucose concentration. To achieve a linear relationship with glucose concentration or its logarithm with different proportions of O_2 , it was determined experimentally that an enzyme ratio of BOD to FAD-GDH in the range of approximately $120 \pm 10 \text{ mU}_{BOD} \cdot U_{FAD-GDH}^{-1} \cdot \text{atm}_{O_2}^{-1}$ is required. Results concerning glucose biosensing under air conditions are detailed in the Supporting Material (Part 12)

Exploring Current Dynamics in the Electroless Glucose–Oxygen Bioconversion. Following the development of the glucose biosensor, the second focus in this research shifted toward the study of the electrical current resulting from the coupling of glucose oxidation with O_2 reduction, particularly at OCP where the current is equal to 0 ($I_{\rm glucose\ oxidation} = I_{\rm O2\ reduction}$). In this study, our experimental parameters were aligned with conditions of 100% O_2 and a glucose concentration of 10 mM.

Table 1 presents data from a series of experiments investigating the bioconversion current (in μ A·cm⁻²) of bulk

Table 1. OCP (V) after the Addition of 10 mM Glucose and the Bioconversion Current I (μ A·cm⁻²) at the Applied OCP for Different Experiments with Different Amounts of FAD-GDH and BOD^a

			()	/ -25
experiment	FAD-GDH (U)	BOD (U)	OCP (V)	$I (\mu A \cdot cm^{-2})$
(a)	8.100	0.130	0.150	60 ± 4
(b)	8.100	0.097	0.090	20 ± 6
(c)	8.100	0.065	0.070	15 ± 3
(e)	8.100	0.032	0.010	05 ± 1
(f)	6.075	0.097	0.165	61 ± 4
(g)	4.050	0.065	0.162	45 ± 2
(h)	2.025	0.032	0.163	25 ± 9
(i)	6.075	0.130	0.190	65 ± 7
(j)	4.050	0.130	0.230	55 ± 4
(k)	2.025	0.130	0.260	46 ± 1

^aAll experiments were carried out with 100 mM PBS (pH 7.4), under 100% O₂, at room temperature, and using GCE as the working electrode.

electrolysis carried out at OCP after the addition of 10 mM glucose and under 100% O₂. The experiments are carried out at room temperature using a glassy carbon.

With the potential range for the coupling of reactions being between 0.04 and 0.31 V as obtained from overlaid CV experiments of BOD@FcMe₂-LPEI and GDH@FcMe₂-LPEI in the presence of O₂ and glucose, respectively (Figure S17), the midpoint of this range is approximately 0.17 V. The best coupling, therefore, would be expected if OCP falls within ± 50 mV of this midpoint. This means the OCP, mainly depending on the amount of both enzymes, should ideally be between 0.12 and 0.22 V for optimal reaction coupling.

For a fixed concentration of FAD-GDH (8.100 U), BOD concentration was decreased sequentially from 0.032 U in experiment (a) to 0.130 U in experiment (e). This gradient allows us to observe the effect of BOD concentration on OCP and the bioconversion current. The OCP values range from 0.150 V in experiment (a) to 0.010 V in experiment (e). The highest bioconversion current (60 \pm 4 $\mu \text{A} \cdot \text{cm}^{-2}$) is observed with the highest BOD concentration (0.130 U) and a relatively higher OCP (0.150 V), indicating that this condition might be closer to the optimal operating conditions for this electrochemical system.

On the other hand, for a fixed concentration of BOD (0.130 U), the concentration of FAD-GDH was varied across the experiments. It is highest in experiment (a) at 8.100 U and lowest in experiment (k) at 2.025 U. The OCP values range from 0.150 V in experiment (a) to 0.260 V in experiment (k), showing an increasing trend as the concentration of FAD-GDH decreases. The bioconversion current varies, with the highest value in experiment (i) at 65 \pm 7 $\mu\text{A}\cdot\text{cm}^{-2}$ and the lowest in experiment (k) at 46 \pm 1 $\mu\text{A}\cdot\text{cm}^{-2}$. The bioconversion current does not show a simple correlation with either FAD-GDH or BOD concentrations. However, experiment (i), with a reduced FAD-GDH concentration (6.075 U) compared to (a) (8.100 U) but the same BOD concentration, shows a slightly higher bioconversion current.

In a last set of experiments, the ratio between the enzymes FAD-GDH and BOD was kept constant, and the absolute concentration of each enzyme was varied. Based on this setup, we can analyze the influence of enzyme concentration on OCP and the bioconversion current (I) (Experiments (a), (f), (j), and (k) in Table 1).

Despite variations in enzyme concentrations while keeping the same ratio between both enzymes amount, the OCP remains relatively stable across the experiments. As the absolute concentrations of both enzymes decrease, there is a noticeable reduction in the bioconversion current. This trend indicates that while the OCP remains fairly stable, the current is dependent on the total enzymatic activity present in the system. With lower amounts of enzymes, the system's capacity to catalyze the glucose oxidation and O_2 reduction reactions diminishes, resulting in a lower current. This sensitivity is evident in the decrease in current from $60 \pm 4 \,\mu\text{A}\cdot\text{cm}^{-2}$ in experiment (a) with the highest enzyme concentrations to 25 \pm 9 $\mu\text{A}\cdot\text{cm}^{-2}$ in experiment (h) with the lowest.

In conclusion, the experiments illustrate that OCP is a key parameter influencing the bioconversion current within this duo enzymatic electrochemical system. The OCP is determined by the interplay between the concentrations of the enzymes FAD-GDH and BOD, as well as the availability of the substrates, glucose, and O_2 . The data suggests that for a given ratio of enzymes, when the concentration of both glucose and O_2 is kept constant, the bioconversion current is directly proportional to the amount of enzyme present. An increase in the concentration of both enzymes leads to an increase in the bioconversion current, while a decrease in enzyme concentration results in a lower current.

In experiment (i) from Table 1 that yielded the higher bioconversion current, the bioconversion of glucose was investigated through a bulk electrolysis experiment conducted at OCP of 0.190 V. The experimental procedure involved altering the atmospheric conditions in a sequential manner, starting with N_2 to establish a baseline, then switching to O_2 ,

ACS Sensors pubs.acs.org/acssensors Article

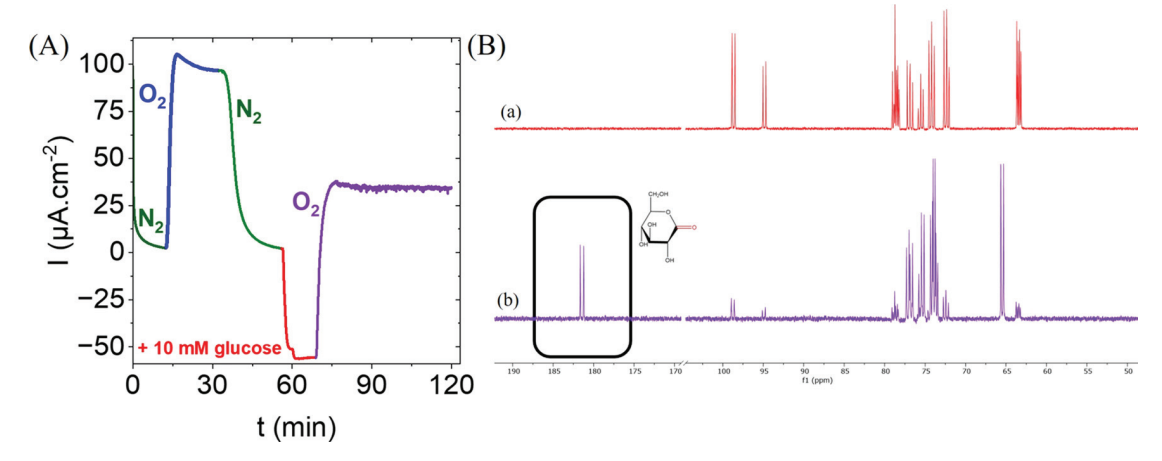


Figure 4. (A) Bulk electrolysis experiment carried out at the OCP (0.19 V), which correlates with the addition of 10 mM 13 C glucose and in the presence of O_2 . This was initially performed under N_2 , followed by O_2 , then reverted to N_2 . Subsequently, 10 mM glucose was introduced, and finally, the atmosphere was switched back to O_2 . (B) 13 C glucose NMR analysis (a) before and (b) 24 h after bulk electrolysis. This experiment was carried out with 100 mM PBS (pH 7.4), under O_2 , at room temperature, and using GCE as the working electrode.

reverting back to N_2 , introducing 10 mM glucose under N_2 , and finally returning to an O_2 atmosphere (Figure 4A).

The experiment starts under a nitrogen atmosphere to create an O_2 -free environment. The initial current is likely baseline or background current due to any residual electroactive species or the electrode process itself. When O_2 is introduced, there is a noticeable current response where the current reached 100 ± 2 $\mu\text{A}\cdot\text{cm}^{-2}$. This change indicates that the system is sensitive to the presence of O_2 , which is involved in the electroenzymatic reduction of O_2 catalyzed by BOD. Reverting to a N_2 atmosphere, the current decreases and returned to the baseline.

The addition of 10 mM 13 C-labeled glucose leads to a sharp increase in current, which peaks at 65 \pm 7 μ A·cm $^{-2}$. This current represents the oxidation of glucose. Finally, returning to an O_2 atmosphere after glucose addition seems to stabilize the current at a level lower than the initial O_2 introduction, indicating a sustained reaction involving both O_2 and the now-present glucose.

The bioconversion current attributable to glucose oxidation and O_2 reduction is determined by calculating the difference in the absolute current values before and after the introduction of glucose, under the O_2 atmosphere and corresponding to $65 \pm 7~\mu \text{A} \cdot \text{cm}^{-2}$. Following 24 h of bulk electrolysis, ¹³C NMR spectroscopic analyses were conducted to ascertain the formation of gluconolactone. The ¹³C NMR spectra were initially recorded for the glucose solution prior to electrolysis to establish a baseline reference (Figure 4B, spectra (a)). Subsequently, postelectrolysis, the ¹³C NMR spectra were acquired ((Figure 4B, spectra (b))).

Alongside the typical peaks for glucose, we were able to discern additional peaks indicative of gluconolactone formation. Gluconolactone, being a cyclic ester derived from glucose, exhibits a characteristic peak corresponding to the carbonyl carbon resulting from the oxidation of the aldehyde group in glucose. This peak is typically found significantly downfield, often between 160 and 180 ppm, due to the electron-withdrawing effect of O₂ in the ester linkage.

To evaluate the efficacy of the electroless coupling of glucose oxidation to O_2 reduction in the synthesis of gluconolactone, we meticulously replicated experiments (e) and (i) as outlined in Table 1 without any applied potential. These experiments were specifically chosen for their relevance in demonstrating

the bioconversion currents under varying voltage conditions. In experiment (e), a current of $5 \pm 1~\mu \text{A} \cdot \text{cm}^{-2}$ was achieved at 0.01 V, while experiment (i) yielded a current of $65 \pm 7~\mu \text{A} \cdot \text{cm}^{-2}$ at 0.19 V. Both sets of conditions were maintained under a constant O_2 flow of 0.5 mL·min⁻¹, in the presence of a 10 mM concentration of ^{13}C -labeled glucose, and without any applied potential.

Upon analysis after 24 h, the ¹³C NMR spectra confirmed the optimization that was done. For the experiment replicated as per (i) in Table 1, the ¹³C NMR results exhibited the characteristic peak of gluconolactone (Figure S18B), a clear indication that the electroless process was effective under these specific experimental conditions. Conversely, for experiment (e), the ¹³C NMR spectrum revealed only a low-intensity peak corresponding to gluconolactone (Figure S18A). Additionally, the comparison of the intensity peaks corresponding to gluconolactone production with an applied potential (Figure 4B) and with the electroless system (Figure S18) showed that the production of gluconolactone is of the same order of magnitude in both systems. These results not only confirm the production of gluconolactone through the electroless coupling but also highlight the influence of both enzymes amount on the yield and efficiency of the bioconversion process.

CONCLUSIONS

In conclusion, this work illustrated the coupling of glucose oxidation to $\rm O_2$ reduction both catalyzed by FAD-GDH and BOD, respectively, and utilizing FcMe₂-LPEI as a redox mediator. CV experiments were instrumental in providing that such a coupling is feasible, with both glucose oxidation and $\rm O_2$ reduction transpiring within an overlapping potential range. Additionally, the colocalization of both enzymes on a single electrode did not lead to any observable deactivation, suggesting that the biocatalytic components maintain their functionality even in close proximity.

Subsequently, OCP experiments demonstrated the system's capability to detect a wide range of glucose concentrations in the presence of $\rm O_2$ or air. The meticulous optimization of enzyme concentrations and $\rm O_2$ pressure (120 \pm 10 mU_{BOD}· U_{FAD-GDH}·atm $_{\rm O_2}^{-1}$) were paramount for achieving a linear OCP response with a wide range of glucose concentrations (up to 100 mM). This biosensing system represents a significant

advancement in glucose monitoring technology, with the potential for commercialization. It distinguishes itself through its versatility and simplicity in accurately reading glucose concentrations in a device internal (100% $\rm O_2$) or external (ambient air) to the body.

The final part of this study also revealed that the electroless coupling of the oxidation and reduction reactions was contingent on the OCP, which itself is dependent on the concentrations of both enzymes and the ratio between them as well as the availability of the substrates, O₂, and glucose. By integrating this process into glycogenesis pathways, ³¹ it could disrupt the high glucose and O₂ uptake by tumors. This approach offers a targeted strategy to interfere with tumor metabolism, potentially leading to more effective treatments with reduced side effects. ²⁶

ASSOCIATED CONTENT

Supporting Information

The Supporting Information is available free of charge at https://pubs.acs.org/doi/10.1021/acssensors.4c00685.

 1 H NMR spectrum of synthesized FcMe₂-LPEI; study of the effect of successive additions of 10 μmol of glucose on open circuit potential (OCP); study of the effect of the effect successive additions of 10 μmol of gluconolactone (The product of the reaction) on Open circuit potential (OCP) with FAD-GDH@FcMe₂-LPEI; impact of glucose addition on OCP behavior and the steady state OCP; tracking OCP response over time after successive additions of 4 μmol of glucose with 8.100 U FAD-GDH and 0.008 U BOD (PDF)

AUTHOR INFORMATION

Corresponding Author

Shelley D. Minteer — Department of Chemistry, University of Utah, Salt Lake City, Utah 84112, United States; Kummer Institute Center for Resource Sustainability, Missouri University of Science and Technology, Rolla, Missouri 65409, United States; orcid.org/0000-0002-5788-2249; Email: shelley.minteer@mst.edu

Authors

Wassim El Housseini — Department of Chemistry, University of Utah, Salt Lake City, Utah 84112, United States; Kummer Institute Center for Resource Sustainability, Missouri University of Science and Technology, Rolla, Missouri 65409, United States

Egor Baiarashov — Department of Chemistry, University of Utah, Salt Lake City, Utah 84112, United States; Kummer Institute Center for Resource Sustainability, Missouri University of Science and Technology, Rolla, Missouri 65409, United States

Rokas Gerulskis – Department of Chemistry, University of Utah, Salt Lake City, Utah 84112, United States

Adam Milam – Department of Chemistry, University of Utah, Salt Lake City, Utah 84112, United States

Complete contact information is available at: https://pubs.acs.org/10.1021/acssensors.4c00685

Author Contributions

§W.E.H. and E.B. contributed equally to this work.

Notes

The authors declare no competing financial interest.

ACKNOWLEDGMENTS

This material is based upon work supported by the Chemical Measurement and Imaging program in the National Science Foundation Division of Chemistry under Grant No. CHE-2154206/CHE-2406605, with co-funding from the Biosensing program in the Division of Chemical, Bioengineering, Environmental, and Transport Systems.

REFERENCES

- (1) Brinkert, K.; Mandin, P. Fundamentals and Future Applications of Electrochemical Energy Conversion in Space. *npj Microgravity* **2022**, *8* (1), No. 52, DOI: 10.1038/s41526-022-00242-3.
- (2) Li, M.; Bi, X.; Wang, R.; Li, Y.; Jiang, G.; Li, L.; Zhong, C.; Chen, Z.; Lu, J. Relating Catalysis between Fuel Cell and Metal-Air Batteries. *Matter* **2020**, 2 (1), 32–49.
- (3) Lewis, N. S. Progress in Understanding Electron-Transfer Reactions at Semiconductor/Liquid Interfaces. *J. Phys. Chem. B* **1998**, 102 (25), 4843–4855.
- (4) Reeve, H. A.; Ash, P. A.; Park, H.; Huang, A.; Posidias, M.; Tomlinson, C.; Lenz, O.; Vincent, K. A. Enzymes as Modular Catalysts for Redox Half-Reactions in H₂-Powered Chemical Synthesis: From Biology to Technology. *Biochem. J.* **2017**, 474 (2), 215–230.
- (5) Roy, G.; Gupta, R.; Sahoo, S. R.; Saha, S.; Asthana, D.; Mondal, P. C. Ferrocene as an Iconic Redox Marker: From Solution Chemistry to Molecular Electronic Devices. *Coord. Chem. Rev.* **2022**, *473*, No. 214816.
- (6) Mecerreyes, D.; Porcarelli, L.; Casado, N. Innovative Polymers for Next-Generation Batteries. *Macromol. Chem. Phys.* **2020**, 221 (4), No. 1900490.
- (7) Arechederra, M. N.; Addo, P. K.; Minteer, S. D. Poly (Neutral Red) as a NAD⁺ Reduction Catalyst and a NADH Oxidation Catalyst: Towards the Development of a Rechargeable Biobattery. *Electrochim. Acta* **2011**, *56* (3), 1585–1590.
- (8) Castañeda-Losada, L.; Adam, D.; Paczia, N.; Buesen, D.; Steffler, F.; Sieber, V.; Erb, T. J.; Richter, M.; Plumeré, N. Bioelectrocatalytic Cofactor Regeneration Coupled to CO₂ Fixation in a Redox-Active Hydrogel for Stereoselective C–C Bond Formation. *Angew. Chem., Int. Ed.* **2021**, *60* (38), 21056–21061.
- (9) Hickey, D. P.; Godman, N. P.; Schmidtke, D. W.; Glatzhofer, D. T. Chloroferrocene-Mediated Laccase Bioelectrocatalyst for the Rapid Reduction of O₂. *Electrochim. Acta* **2021**, *383*, No. 138130.
- (10) Taylor, C.; Kenausis, G.; Katakis, I.; Heller, A. "Wiring" of Glucose Oxidase within a Hydrogel Made with Polyvinyl Imidazole Complexed with [(Os-4, 4'-Dimethoxy-2, 2'-Bipyridine) Cl]^{+/2+1}. *J. Electroanal. Chem.* **1995**, 396 (1–2), 511–515.
- (11) Muhs, A.; Bobrowski, T.; Lielpetere, A.; Schuhmann, W. Catalytic Biosensors Operating under Quasi-Equilibrium Conditions for Mitigating the Changes in Substrate Diffusion. *Angew. Chem., Int. Ed.* **2022**, *61* (52), No. e202211559.
- (12) Yuan, M.; Kummer, M. J.; Milton, R. D.; Quah, T.; Minteer, S. D. Efficient NADH Regeneration by a Redox Polymer-Immobilized Enzymatic System. ACS Catal. 2019, 9 (6), 5486–5495.
- (13) Hickey, D. P.; Reid, R. C.; Milton, R. D.; Minteer, S. D. A Self-Powered Amperometric Lactate Biosensor Based on Lactate Oxidase Immobilized in Dimethylferrocene-Modified LPEI. *Biosens. Bioelectron.* **2016**, *77*, 26–31.
- (14) Godman, N. P.; DeLuca, J. L.; McCollum, S. R.; Schmidtke, D. W.; Glatzhofer, D. T. Electrochemical Characterization of Layer-by-Layer Assembled Ferrocene-Modified Linear Poly (Ethylenimine)/Enzyme Bioanodes for Glucose Sensor and Biofuel Cell Applications. *Langmuir* **2016**, 32 (14), 3541–3551.
- (15) Huang, W.; Diaconescu, P. L. Reactivity and Properties of Metal Complexes Enabled by Flexible and Redox-Active Ligands with a Ferrocene Backbone. *Inorg. Chem.* **2016**, 55 (20), 10013–10023.

I

- (16) Hudson, R. D. A. Ferrocene Polymers: Current Architectures, Syntheses and Utility. J. Organomet. Chem. 2001, 637–639, 47–69.
- (17) Lee, I.; Loew, N.; Tsugawa, W.; Ikebukuro, K.; Sode, K. Development of a Third-Generation Glucose Sensor Based on the Open Circuit Potential for Continuous Glucose Monitoring. *Biosens. Bioelectron.* **2019**, 124–125, 216–223.
- (18) Moatti-Sirat, D.; Poitout, V.; Thome, V.; Gangnerau, M. N.; Zhang, Y.; Hu, Y.; Wilson, G. S.; Lemonnier, F.; Klein, J. C.; Reach, G. Reduction of Acetaminophen Interference in Glucose Sensors by a Composite Nafion Membrane: Demonstration in Rats and Man. *Diabetologia* 1994, 37, 610–616.
- (19) Smutok, O.; Katz, E. Biosensors: Electrochemical Devices—General Concepts and Performance. *Biosensors* **2023**, *13* (1), No. 44, DOI: 10.3390/bios13010044.
- (20) Bollella, P.; Katz, E. Biosensors—Recent Advances and Future Challenges. *Sensors* **2020**, *20* (22), No. 6645, DOI: 10.3390/s20226645.
- (21) Milton, R. D.; Lim, K.; Hickey, D. P.; Minteer, S. D. Employing FAD-Dependent Glucose Dehydrogenase within a Glucose/Oxygen Enzymatic Fuel Cell Operating in Human Serum. *Bioelectrochemistry* **2015**, *106*, 56–63.
- (22) Wernert, V.; Lebouin, C.; Benoit, V.; Gadiou, R.; de Poulpiquet, A.; Lojou, E.; Denoyel, R. Direct Electron Transfer of Bilirubin Oxidase at a Carbon Flow-through Electrode. *Electrochim. Acta* 2018, 283, 88–96.
- (23) Logan, B. E.; Zikmund, E.; Yang, W.; Rossi, R.; Kim, K.-Y.; Saikaly, P. E.; Zhang, F. Impact of Ohmic Resistance on Measured Electrode Potentials and Maximum Power Production in Microbial Fuel Cells. *Environ. Sci. Technol.* **2018**, *52* (15), 8977–8985.
- (24) Tekade, R. K.; Sun, X. The Warburg Effect and Glucose-Derived Cancer Theranostics. *Drug Discovery Today* **2017**, 22 (11), 1637–1653.
- (25) Chen, Y.; Cairns, R.; Papandreou, I.; Koong, A.; Denko, N. C. Oxygen Consumption Can Regulate the Growth of Tumors, a New Perspective on the Warburg Effect. *PLoS One* **2009**, 4 (9), No. e7033.
- (26) Grasmann, G.; Smolle, E.; Olschewski, H.; Leithner, K. Gluconeogenesis in Cancer Cells-Repurposing of a Starvation-Induced Metabolic Pathway? *Biochim. Biophys. Acta, Rev. Cancer* **2019**, 1872 (1), 24–36, DOI: 10.1016/j.bbcan.2019.05.006.
- (27) Grist, S. M.; Chrostowski, L.; Cheung, K. C. Optical Oxygen Sensors for Applications in Microfluidic Cell Culture. *Sensors* **2010**, *10* (10), 9286–9316.
- (28) Oughli, A. A.; Ruff, A.; Boralugodage, N. P.; Rodriguez-Maciá, P.; Plumeré, N.; Lubitz, W.; Shaw, W. J.; Schuhmann, W.; Rüdiger, O. Dual Properties of a Hydrogen Oxidation Ni-Catalyst Entrapped within a Polymer Promote Self-Defense against Oxygen. *Nat. Commun.* **2018**, *9* (1), No. 864.
- (29) Etienne, M.; Le, T. X. H.; Nasir, T.; Herzog, G. Electrochemical Filter to Remove Oxygen Interference Locally, Rapidly, and Temporarily for Sensing Applications. *Anal. Chem.* **2020**, 92 (11), 7425–7429.
- (30) Plumeré, N.; Rüdiger, O.; Oughli, A. A.; Williams, R.; Vivekananthan, J.; Pöller, S.; Schuhmann, W.; Lubitz, W. A Redox Hydrogel Protects Hydrogenase from High-Potential Deactivation and Oxygen Damage. *Nat. Chem.* **2014**, *6* (9), 822–827.
- (31) Xu, S.; Minteer, S. D. Enzymatic Biofuel Cell for Oxidation of Glucose to CO₂. ACS Catal. **2012**, 2 (1), 91–94.